

THS 24673302



LIBRA... / Michigan State University

This is to certify that the

thesis entitled

Microstructural Changes in
Boron Doped Ni₃Al During
High Temperature Low Cycle Fatigue
presented by

Yogesh C. Mishra

has been accepted towards fulfillment of the requirements for

Master's of Science degree in Materials Science

Major professor

Date__July 28, 1989

MSU is an Affirmative Action/Equal Opportunity Institution

O-7639

PLACE IN RETURN BOX to remove this checkout from your record. TO AVOID FINES return on or before date due.

DATE DUE	DATE DUE	DATE DUE

MSU Is An Affirmative Action/Equal Opportunity Institution

MICROSTRUCTURAL CHANGES IN BORON DOPED Ni 3Al DURING HIGH TEMPERATURE LOW CYCLE FATIGUE

By

Yogesh Chandra Mishra

A THESIS

Submitted to
Michigan State University
in partial fulfillment of the requirements
for the degree of

MASTER OF SCIENCE

Department of Metallurgy, Mechanics, and Materials Science

1989

ABSTRACT

MICROSTRUCTURAL CHANGES IN BORON DOPED Ni 3Al DURING HIGH TEMPERATURE LOW CYCLE FATIGUE

Ву

Yogesh Chandra Mishra

Microstructural changes in boron doped Ni₃Al during high temperature strain controlled (0.5% and 1% strain amplitudes) and stress controlled (constant stress of 85 MPa) low cycle fatigue were studied. From stress-strain plots, it was found that the true stress (as a function of cumulative strain) showed a maximum, followed by a continuous decrease at large cumulative strain. Extensive grain boundary migration was observed in all but one cyclic tests. Grain boundary migration could be the major softening mechanism. Grain boundary migration was inhibited if the material had dispersion in the form of voids that pin down the grain boundaries.

ACKNOWLEDGEMENTS

I am indebted to my academic adviser, Professor Gunter Gottstein, for his constant encouragement and guidance, and invaluable suggestions throughout this study. I would also like to thank, C. S. Kim, C. S. Lee, Moti Tayal, S. R. Chen, and W. J. Kim for all their valuable help.

Special thanks to the Department of Metallurgy, Mechanics, and Materials Science for providing the necessary facilities for this study, and the financial support in the form of teaching assistantship. Thanks to the Case Center for Computer Aided Design for providing wonderful computing facility.

Finally, the support of U.S. Department of Energy, Office of Basic Science, under grant no. DE-FG02-85ER45205 for the study is gratefully acknowledged.

Table of Contents

LIS	T OF F	IGURES		v
1.	INTRO	DUCTIO	ON	1
2.	LITER	ATURE	SURVEY	3
	2.1	The Ma	terial	3
		2.1.1	Mechanical Properties	3
		2.1.2	Microalloying	5
		2.1.3	Effect of Boron on Grain Boundary Cohesion	5
		2.1.4	Effect of Alloy Stoichiometry	6
		2.1.5	Effect of Testing Environment on the Properties	6
	2.2	Grain B	Soundary Migration During Low Cycle Fatigue	11
3.	EXPE	RIMENT	AL PROCEDURE	16
	3.1	Testing	Material	16
	3.2	Specime	en Preparation	17
		3.2.1	Mechanical Test Specimens	17
		3.2.2	Optical Microscopy Specimens	19
		3.2.3	Scanning Electron Microscopy Specimens	22
	3.3	Mechan	ical Testing	22
		3.3.1	Instron Testing Machine	22

		3.3.2 MTS Testing Machine	24
4.	EXPER	IMENTAL RESULTS	31
	4.1	Mechanical Behavior	31
	4.2	Microstructural Development	36
	4.3	Brittle Failure	36
5.	DISCU	ISSION	47
	5.1	Mechanical Behavior	47
	5.2	Grain Boundary Migration	47
	5.3	Brittle Failure	48
6.	CONC	LUSIONS	49
7.	BIBLIC	OGRAPHY	51

LIST OF FIGURES

Figure Captions	Page
Fig. 1. Yield stress as a function of test temperature for Ni ₃ Al-base	
aluminide alloys, Hastelloy, and type 316 stainless steel.	4
Fig. 2. Effect of stoichiometry on fracture mode of B-doped Ni 3Al	
at room temperature.	7
Fig. 3. Plastic strain to fracture (%) of rapidly solidified Ni ₃ Al-B	
as a function of Al and B concentration. The solid lines	
indicate constant NiAl ratio (at. %).	8
Fig. 4. Effect of stoichiometry on grain boundary segregation (in	
terms of peak-height ratio) and room temperature tensile	
ductility of B-doped Ni ₃ Al containing 24 to 25.2 at. % Al.	9
Fig. 5. Plot of tensile elongation of Ni ₃ Al alloys as a function	
of (Al+Hf) concentration for bare specimens tested at 600°C	
in vacuum or for specimens preoxidized at 1100°C/2h +	
850°C/5h and tested in air. Solid symbols for alloys with	
0.5% Hf and open symbols for the alloy without Hf.	10
Fig. 6. SEM micrograph showing cyclic grain boundary migration after	
testing for 15 cycles in reverse bending at a frequency of	
0.17 Hz and a strain amplitude of $\pm 0.28\%$. A pre-existing	

Figure Captions	Page
twin is at A, and B marks the initial position of the boun-	
dary prior to testing.	12
Fig. 7. Two-beam interferometer (monochromic light) showing repetitive	
cyclic markings and the presence of sliding after testing for	
3 cycles in reverse bending at a frequency of 0.10 Hz and a	
strain amplitude of $\pm 0.48\%$.	13
Fig. 8. Optical micrograph, using Nomarski interference contrast,	
showing the presence of a fine structure within the migra-	
tion markings after testing for 8 cycles reverse bending at a	
frequency of 0.17 Hz and a strain amplitude of $\pm 0.28\%$.	14
Fig. 9. Fatigue Sample (B-doped Ni 3Al).	18
Fig. 10. Microstructure of Ni ₃ Al annealed at 800°C for 5 hour.	20
Fig. 11. Microstructure of Ni ₃ Al annealed at 800°C for 5 hour.	21
Fig. 12. Instron testing machine set up.	23
Fig. 13. Computerized high temperature high vacuum servo-	
hydraulic test system.	25
Fig. 14. High temperature grip assembly.	26
Fig. 15. Specimen inserts for the high temperature high vacuum	
MTS test system.	28
Fig. 16. Final set up inside the vacuum furnace of the	
high temperature high vacuum MTS test system.	29
Fig. 17. Plot of true stress versus cumulative strain for 0.5% strain	

	Figure Captions	Page
	amplitude cyclic deformation in high vacuum at 600°C.	32
Fig. 18	. Plot of true stress versus cumulative strain for 1% strain	
	amplitude cyclic deformation in reducing atmosphere of	
	$(90\% N_2 + 10\% H_2)$ at 600° C.	33
Fig. 19	Plot of true stress versus number of cycles for 1% strain	
	amplitude cyclic deformation in reducing atmosphere of	
	$(90\% N_2 + 10\% H_2)$ at 600° C.	34
Fig. 20	. Plot of true stress versus cumulative strain for constant	
	stress controlled test, using constant stress of 85 MPa, in	
	reducing atmosphere of (90% $N_2 + 10\% H_2$) at 600° C.	35
Fig. 21	. Microstructure of Ni ₃ Al, in the plane perpendicular to	
	the loading axis, annealed at 800°C for 5 hour, after 100	
	cycles of 0.5% strain amplitude at 600°C.	37
Fig. 22	2. Microstructure of Ni ₃ Al, in the plane perpendicular to	
	the loading axis, annealed at 800°C for 5 hour, after 3900	
	cycles of 1% strain amplitude at 600°C.	38
Fig. 23	3. Microstructure of Ni ₃ Al, in the plane perpendicular to	
	the loading axis, annealed at 800°C for 5 hour.	39
Fig. 24	1. Microstructure of Ni ₃ Al, in the plane perpendicular to	
	the loading axis, annealed at 800°C for 5 hour, after 790	
	cycles of constant stress of 85 MPa at 600°C.	40
Fig 25	Microstructure of Ni Al in the plane perpendicular to	

		Figure Captions	Page
		the loading axis, annealed at 1200°C for 2 hour.	41
Fig.	26.	Microstructure of Ni ₃ Al, in the plane perpendicular to	
		the loading axis, annealed at 1200°C for 2 hour, after 1000	
		cycles of 0.5% strain amplitude at 600°C.	42
Fig.	27.	Microstructure of Ni ₃ Al, in the plane parallel to	
		the loading axis, annealed at 800°C for 5 hour, after 100	
		cycles of 0.5% strain amplitude at 600°C.	43
Fig.	28.	Microstructure of Ni ₃ Al, in the plane parallel to	
		the loading axis, annealed at 1200°C for 2 hour, after 1000	i
		cycles of 0.5% strain amplitude at 600°C.	44
Fig.	29.	SEM micrograph of the fractured surface of a specimen broken	
		during cyclic loading in the (90% N_2 + 10% H_2) atmo-	
		sphere.	45
Fig.	30.	SEM micrograph of the fractured surface of a specimen broken	
		during cyclic loading in the (90% $N_2 + 10\% H_2$) atmosphere.	46

1. INTRODUCTION

Intermetallic compound Ni₃Al forms Ll₂ type ordered crystal structure below the peritectic temperature [1]. Ni₃Al has good high temperature strength, and oxidation and corrosion resistance [2]. Unlike the most conventional alloys, the yield strength of Ni₃Al increases with the increasing temperature [3-5]. Single crystals of Ni₃Al are ductile where as polycrystalline Ni₃Al is brittle at ambient temperatures [6-10]. The ductility of polycrystalline Ni₃Al significantly improves with the small additions of boron [8] and careful control of aluminum content [11-13].

The superior high temperature properties and fabricability of boron doped Ni₃Al makes it an attractive candidate for the high temperature structural applications. In the high temperature applications, the material is likely to be subjected to cyclic loading due to vibrations etc. Generally, the materials subjected to the high temperature cyclic loading under go microstructural changes leading to the degradation of properties that may result in the failure of the structure.

It is well known that the high temperature deformation may cause recrystallization and/or grain growth phenomena in alloys that cause softening of the materials. Grain boundary migration during high temperature fatigue has been observed in Pb [14,15], Al [16,17], and Ni [18].

The current study is to elucidate the microstructural changes during high temperature low cycle fatigue. This study would provide a better understanding of the behavior of the boron doped Ni₃Al, during low cycle fatigue, for the high temperature structural applications.

2. LITERATURE SURVEY

2.1 The Material

2.1.1 Mechanical Properties

Long range ordered crystal structures have attractive properties for the high temperature structural applications. Many L1₂ compounds show increase in flow stress with the increasing temperature [20-21]. Ni₃Al falls in this category of compounds and shows increasing strength, up to 600° C, with the increasing temperature [Fig. 1.] [19]. Ni₃Al (γ' phase) is the strengthening constituent of commercial nickel base super-alloys. It provides high temperature strength and creep resistance to the super-alloys.

Although single crystals of Ni₃Al are ductile, the polycrystalline Ni₃Al is brittle at both room temperature and at high temperatures [22]. The grain boundaries of polycrystalline Ni₃Al are intrinsically brittle [23,24] and the material fractures in the intergranular mode.

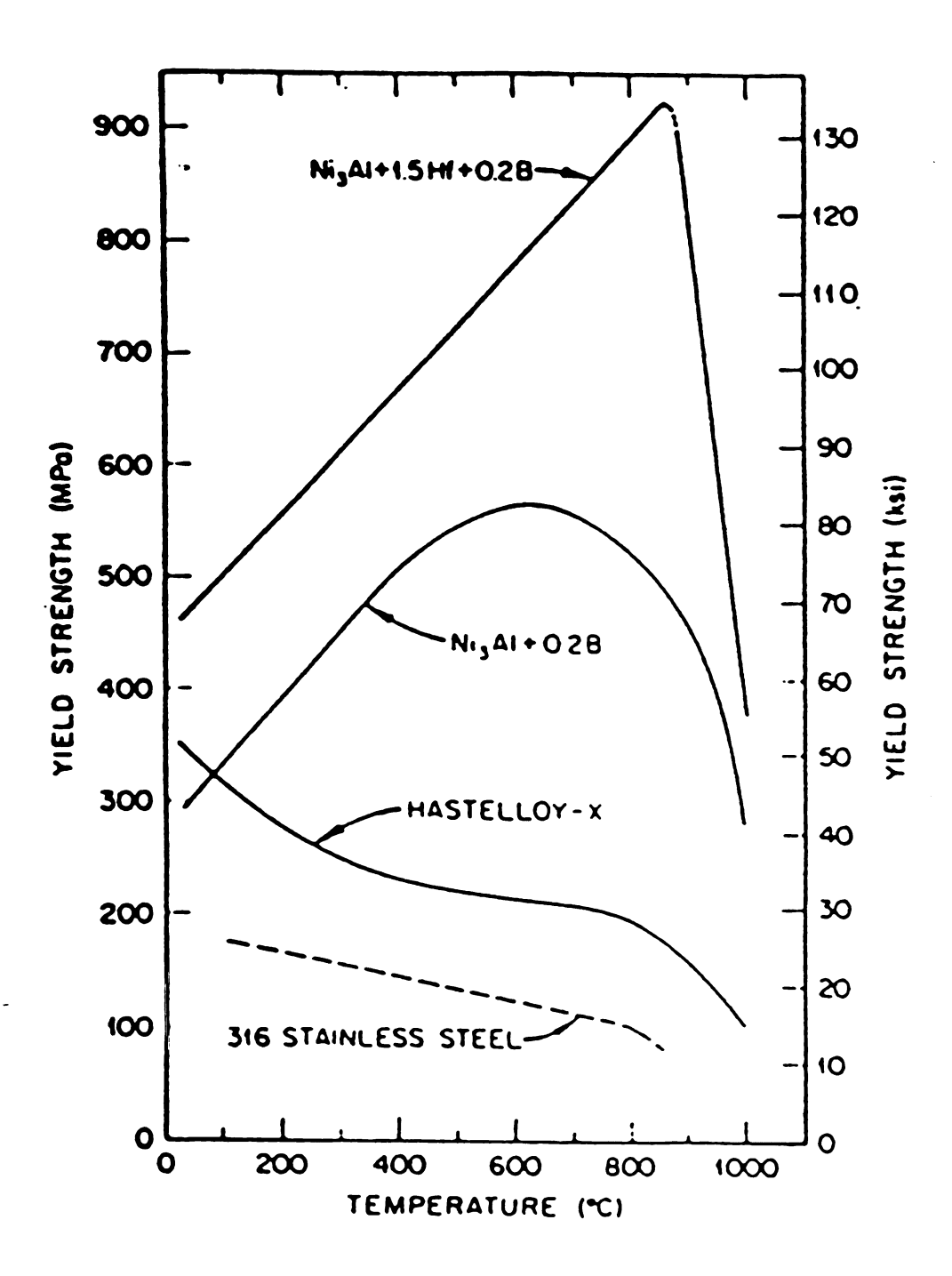


Fig. 1. Yield stress as a function of test temperature for Ni_3 Al-base aluminide alloys, Hastelloy, and type 316 stainless steel [19].

2.1.2 Microalloying

Small additions (in the ppm range) of dopants can increase the grain boundary cohesion in the polycrystalline Ni_3Al . Boron was found to be most effective dopant in improving the ductility and fabricability of the polycrystalline Ni_3Al [11,22,25]. Taub, Huang and Chang [13] reported the beneficial effect of boron by testing Ni_3Al foil prepared by melt spin technique. With the increasing boron content, the yield strength sharply increases and the ductility gradually falls [19]. Detrimental $Ni_{20}Al_3B_6$ phase starts to precipitate as the boron content is increased beyond 0.3 wt. % [12].

2.1.3 Effect of Boron on Grain Boundary Cohesion

With the small additions of boron, the mode of fracture in the polycrystalline Ni₃Al changes from intergranular to a mixture of transgranular and intergranular fracture [12]. Boron segregates at the grain boundaries [19] and eases the accommodation of slip. It improves the mobility of grain boundary dislocations which are left behind when lattice distortion which enters the boundary from one side and leaves it from other [26-27]. Thus the transmission of slip from grain to grain is possible and the polycrystals, otherwise brittle, become ductile [28].

2.1.4 Effect of Alloy Stoichiometry

The beneficial effect of boron in the polycrystalline Ni₃Al is very sensitive to the stoichiometry of the alloy [11,22]. By careful control of Aluminum concentration and thermo-mechanical treatment, Liu et al. [22] reported tensile elongation greater than 50% and virtually transgranular fracture in Ni-24 at. % Al + 0.02-0.10 wt. % B alloy.

Boron is most effective in improving ductility and promoting transgranular fracture in Ni₃Al containing 24 at. % Al [Figs. 2-4] [19].

2.1.5 Effect of Testing Environment on the Properties

In boron doped Ni₃Al alloys, the tensile ductility strongly depends on the testing environment, with much lower ductility in air than in vacuum at 600°C [Fig. 5.] [2]. The loss of ductility is accompanied by a change in fracture mode from transgranular to intergranular. The embrittlement is due to a dynamic effect that simultaneously involves localized stress concentrations, gaseous oxygen, and high temperature [2]. The severity of environmental effect on the high temperature ductility is affected by preoxidation in air as well as by the aluminum content of the alloy. The oxygen embrittlement becomes less severe with a decrease in aluminum concentration from 24 to 21 at.%.







(a) 24% AI, ∈ = 49.4% TRANSGRANULAR FRACTURE

(b) 24.5 % AI, € = 37.0 % MIXED FRACTURE MODE

(c) 25.0% AI, €= 6.0% INTERGRANULAR FRACTURE

Fig. 2 Effect of stoichiometry on fracture mode of B-doped Ni_3Al at room temperature [19].

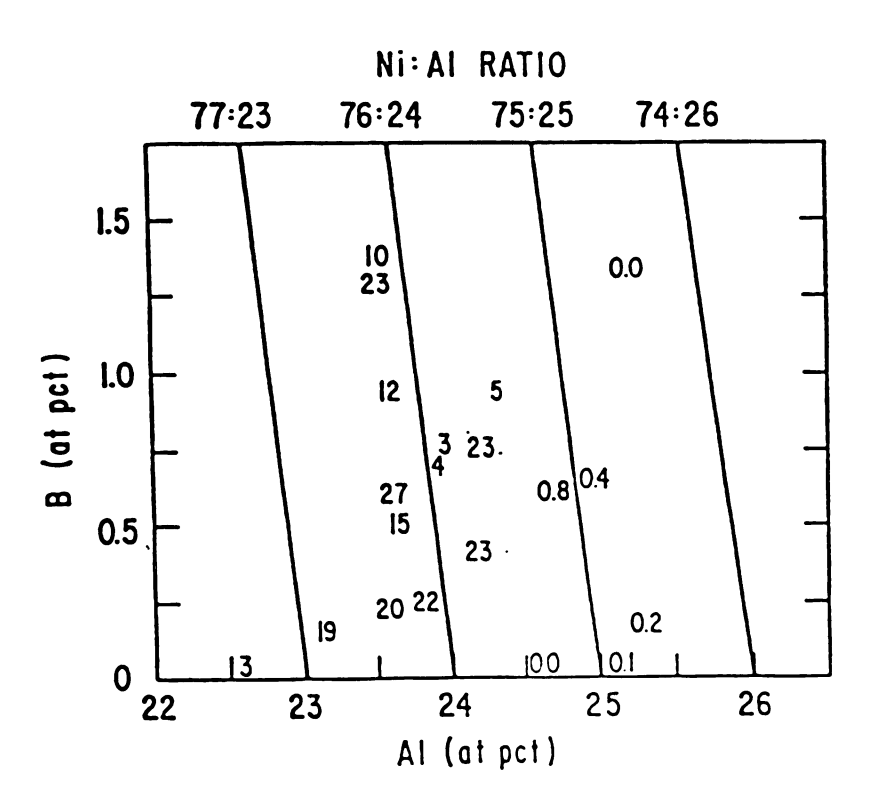


Fig. 3. Plastic strain to fracture (%) of rapidly solidified Ni_3 Al-B as a function of Al and B concentration. The solid lines indicate constant NiAl ratio (at. %) [19].

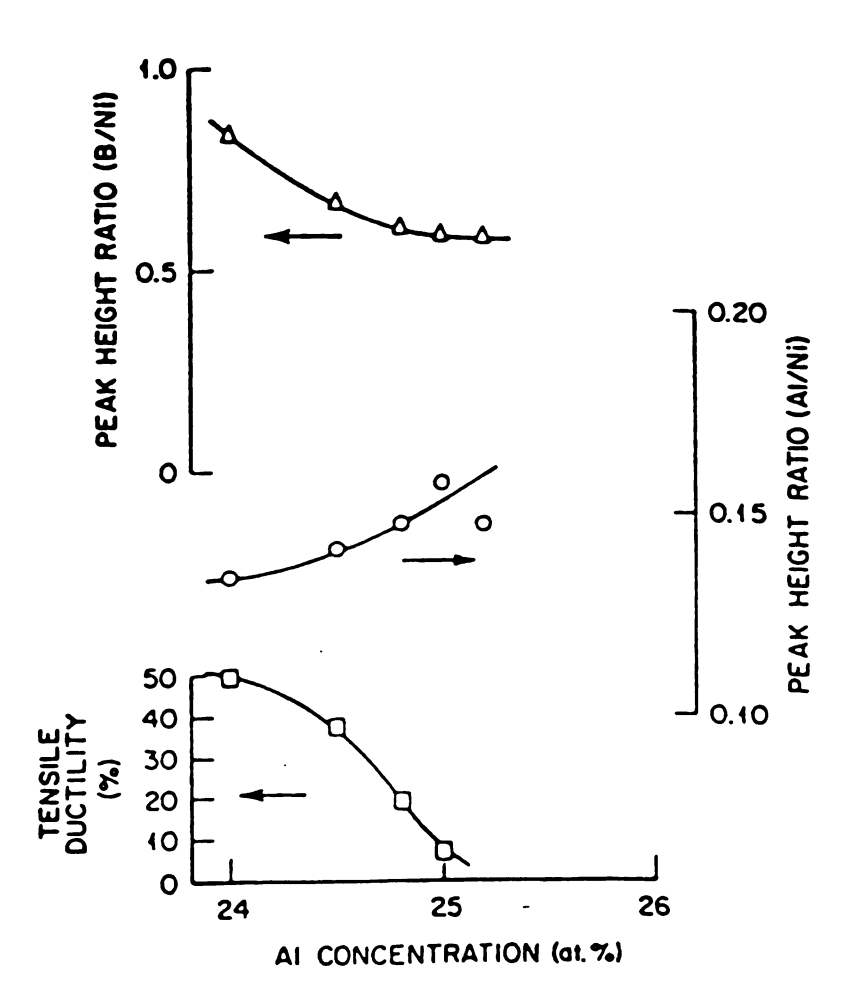


Fig. 4. Effect of stoichiometry on grain boundary segregation (in terms of peak-height ratio) and room temperature tensile ductility of B-doped Ni_3Al containing 24 to 25.2 at. % Al [19].

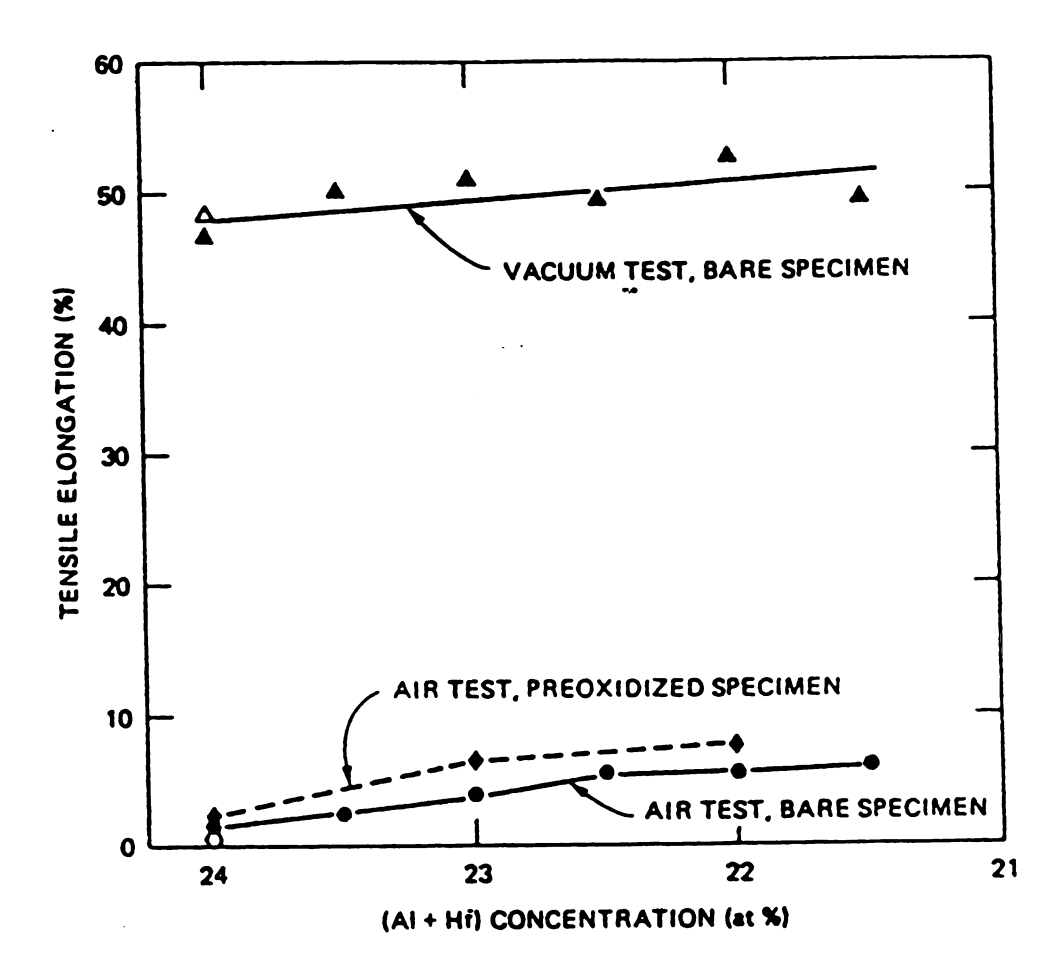


Fig. 5. Plot of tensile elongation of Ni_3 Al alloys as a function of (Al+Hf) concentration for bare specimens tested at 600° C in vacuum or for specimens preoxidized at 1100° C/2h + 850° C/5h and tested in air. Solid symbols for alloys with 0.5% Hf and open symbols for the alloy without Hf [2].

2.2 Grain Boundary Migration During Low Cycle Fatigue

Grain boundary migration during high temperature fatigue is an important microstructural phenomenon. Snowden [29] first reported the grain boundary migration and the appearance of slip trace in the bending fatigue test of pure lead. He found that the grain boundaries tend to migrate to positions $\pm 45^{\circ}$ to the specimen axis that resulted in the formation of an orthogonal grain structure. After large number of cycles, the rate of migration decreased possibly due to the alignment of grain boundaries in the directions of maximum shear stress.

Grain boundary migration and grain boundary sliding have been reported in Al[16,17,30], Pb[14,15], Pb-Sn solid solution alloy[31,32], Al-Mg solid solution alloy[33], and Ni[18]. Room temperature reverse bending and torsion fatigue of the high purity lead (99.9995%) showed microstructural changes right from the first cycle. The result showed extensive grain boundary migration and as result a series of parallel markings at many boundaries could be observed under optical microscope [Fig. 6.] [14,15]. A well defined one-to-one correspondence between the number of grain boundary markings and the total number of cycles was observed. The clarity of each migration marking suggests cyclic grain boundary sliding which was confirmed using two-beam interferometry [Fig. 7.] [14,15]. Optical microscopy, using Nomarski interference contrast, revealed a fine structure within the migration markings [Fig. 8.] [14,15]. In coarse grained specimens, the longer grain boundaries formed a zig-zag pattern of migration markings.

Abdel-Raouf et al. [34] reported a change in the grain morphology in OFHC Cu due to the grain boundary migration during cyclic test at 650°C at a low

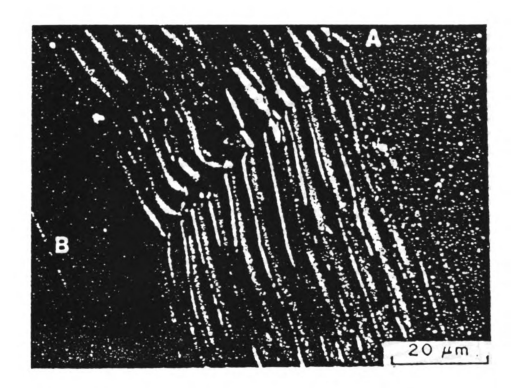


Fig. 6. SEM micrograph showing cyclic grain boundary migration after testing for 15 cycles in reverse bending at a frequency of 0.17 Hz and a strain amplitude of $\pm 0.28\%$. A pre-existing twin is at A, and B marks the initial position of the boundary prior to testing [14,15].

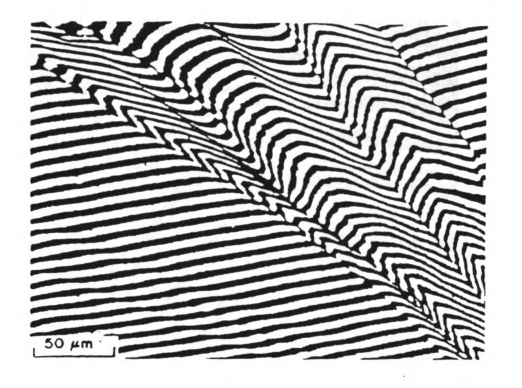


Fig. 7. Two-beam interferometer (monochromic light) showing repetitive cyclic markings and the presence of sliding after testing for 3 cycles in reverse bending at a frequency of 0.10 Hz and a strain amplitude of $\pm 0.48\%$ [14,15].

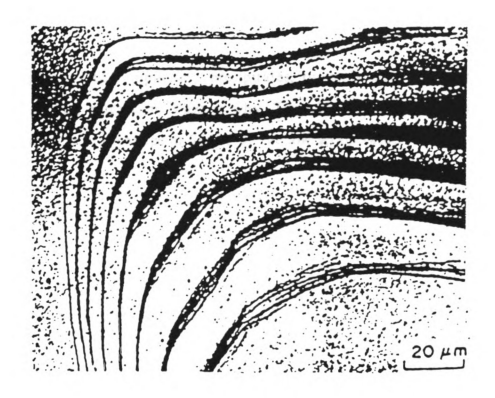


Fig. 8. Optical micrograph, using Nomarski interference contrast, showing the presence of a fine structure within the migration markings after testing for 8 cycles reverse bending at a frequency of 0.17 Hz and a strain amplitude of ± 0.28% [14,15].

strain rate ($4 \times 10^{-4} \ s^{-1}$). The grain shape was found to be strain rate dependent with no change in the grain morphology at high strain rates. Snowden, and Langdon et al. proposed that the grain boundary migration was stress induced process. Recently, Chen [35] proposed that the grain boundary migration is strain induced phenomenon.

Dispersions like impurities, precipitates, or voids slow down or inhibit the grain boundary migration. That is why, Type 304 stainless steel does not show any microstructural change at 760°C at the low strain rates.

3. EXPERIMENTAL PROCEDURE

3.1 Testing Material

A bar shaped casting prepared by arc-melting several times in argon atmosphere to promote homogeneity and then drop-cast in a copper mold was supplied by Oak Ridge National Lab. The final composition of the casting was as follows:

Ni: 76 at. %

Al: 24 at. %

B: 0.24 at. %

One lot of material was received three years back and the another lot was received one year back. After vacuum annealing, the earlier lot showed a smaller grain size as compared to the latter lot. This point would be brought up in the heat treatment section.

3.2 Specimen Preparation

3.2.1 Mechanical Test Specimens

(1) Ni₃Al cyclic test samples were machined from the blocks cut from the supplied cast bars. The blocks were annealed in a vacuum furnace at 800°C for 3 hour so as to ease the machining of the material. Specimens were machined to the shape and dimensions as shown in Fig. 9. [35].

(2) Heat Treatment

All the specimens were annealed in a vacuum furnace at a pressure of approximately 10^{-3} Pa at 800^{0} C for 5 hour except for one sample which was annealed at 1200^{0} C for 2 hour. Annealed specimens were chemically polished at 60^{0} C to remove any surface irregularity, using the following solution:

Nitric Acid: 20 ml

Phosphoric Acid: 20 ml

Distilled Water: 20 ml

Acetic Acid: 10 ml

Hydrofloric Acid: 10 ml

Hydrochloric Acid: 10 ml

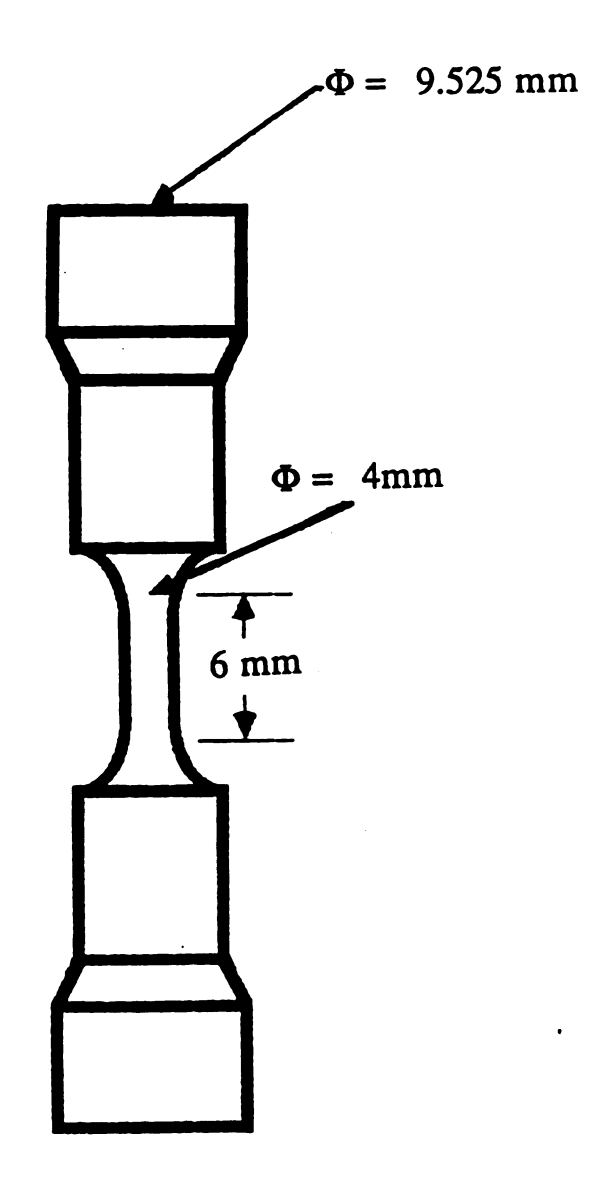


Fig. 9. Fatigue Sample (B-doped Ni_3Al) [35].

19

The two batches of Ni₃Al were received two years apart. The grain size of

the heat treated specimens from earlier batch was small and grains were equi-axial

[Fig. 10.] where as the grain size of latter batch was larger and the microstructure

was dendritic [Fig. 11.]. This difference can be explained as some variation in

fabrication procedure of the material.

3.2.2 Optical Microscopy Specimens

After the completion of cyclic tests, some micrographs were taken by polish-

ing the plane parallel to the loading direction. Specimens were cut perpendicular

to the loading direction with a slow diamond wheel cutting machine (Buehler

Isomet). Subsequently, they were mounted in cold setting resin and polished on

abrasive grit paper and then on a cloth by alumina powder to get a mirror like

surface. The polished samples were etched with the following solution:

CuSO₄: 5g

- 0

HCl:

20 ml

H₂O:

20 ml

All the optical micrographs were taken with a Neophot 21 Microscope.

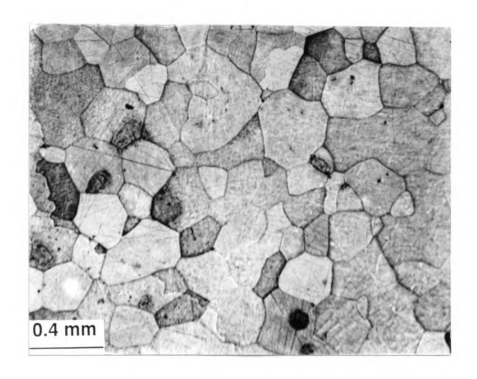


Fig. 10. Microstructure of Ni_3Al annealed at $800^{\circ}C$ for 5 hour.

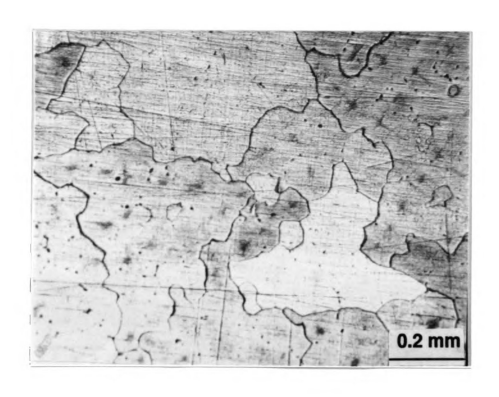


Fig. 11 Microstructure of Ni₃Al annealed at 800°C for 5 hour.

3.2.3 Scanning Electron Microscopy Specimens

The fractured surface was ultrasonically cleaned with acetone. A Hitachi SEM was used to study the fractured surface. The applied voltage was 25kV.

3.3 Mechanical Testing

Two different testing machines and set-up were used to perform the high temperature low cycle fatigue tests.

3.3.1 Instron Testing Machine

High temperature low cycle fatigue tests were conducted on a floor model electro-mechanical Instron testing machine with a 500 Kg tension-compression reversible load cell. The pull rods and button grips were made of 310 heat resistant stainless steel. To avoid the oxidation of the specimen, during high temperature testing, a cylindrical protective chamber was designed as shown in Fig. 12. [35]. A stainless steel ring with a clearance of 0.75 mm to pull rod was welded at the top of the tube, while the lower ring which fitted to the lower pull rod was made of Invar and the dimensions were chosen such that at temperature higher than 200°C, a tight fit with the lower pull rod was obtained due to the difference in the thermal expansion between the Invar ring and lower pull rod.

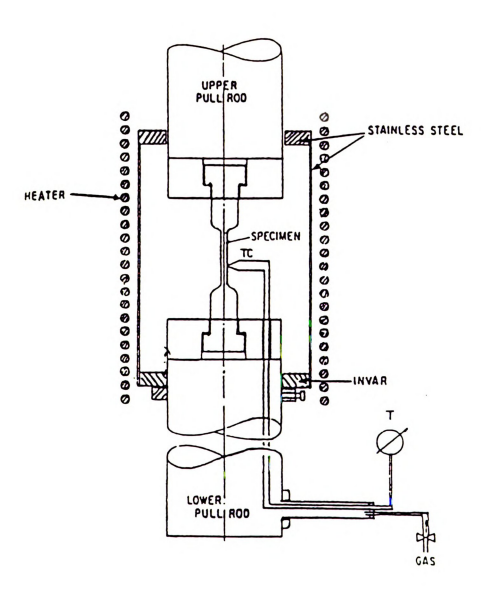


Fig. 12. Instron testing machine set up [35].

During the test, a reducing gaseous mixture (90% $N_2 + 10\% H_2$) was flown at the flow rate of 12 liter/hour at 5 psi to minimize the oxidation. Higher flow rates were avoided to reduce burning of the gas at the top of the chamber and the unwanted back pressure.

Computer codes were developed to computer control the Instron by digital output from IBM XT personal computer and for data acquisition of load cell signals using an A/D converter. Load and displacement data from test could be stored at chosen interval. The resolution of data acquisition was 4 μ m per data set with a accuracy better than 0.1%.

3.3.2 MTS Testing Machine

In the later part of the project a new computerized high temperature high vacuum servohydraulic test system was used. The essential parts of the system are schematically shown in Fig. 13. [35]. The system includes a closed loop frame (MTS 810) with 10-100 kN (MTS 661.20A-03) or 0.5-10kN (MTS 661.19) load cell, a 25.4 mm gauge length water cooled high temperature extensometer with maximum strain range of 30% and minimum strain range of -10%, and a Centorr S-60 high vacuum high temperature furnace. The maximum resolution of the extensometer is 0.1 μ m, however, due to limitation of 12 bit A/D converter the resolution is 0.488 μ m.

Specially designed grips [Fig. 14.] [35] were used to avoid the crossover phenomenon during change in the loading direction in tension-compression fatigue

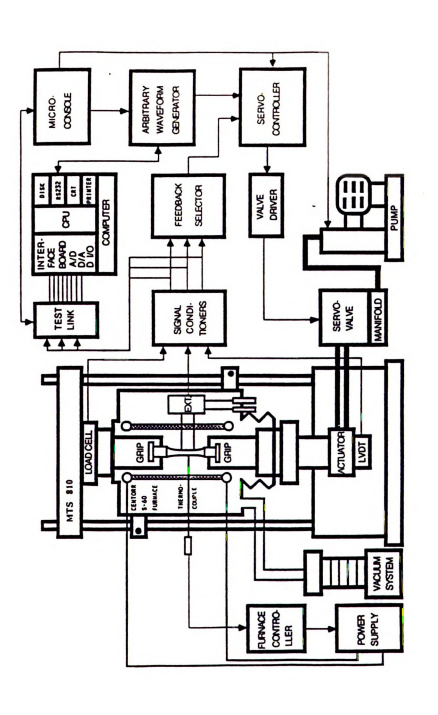


Fig. 13. Computerized high temperature high vacuum servohydraulic test system [35].

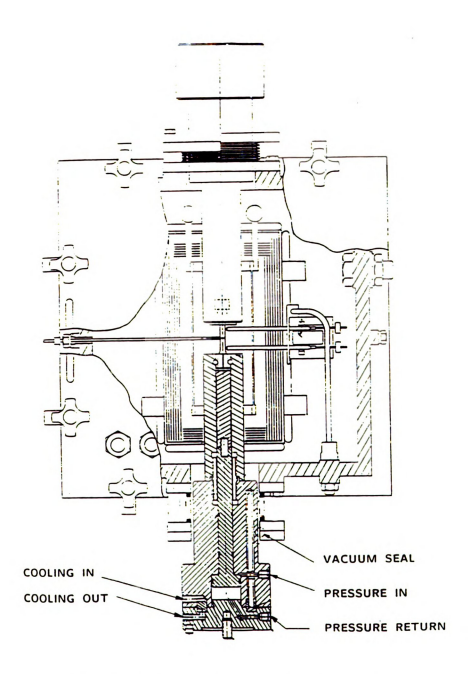


Fig. 14. High temperature grip assembly [35].

test. The two ends of the specimen were preloaded by applying hydraulic pressure on the pistons residing inside the pull rods. The specimen insert included two pair of collets, four tungsten pins and two extension pistons shown in Fig. 15 [35]. All the hot zone parts are made of high temperature molybdenum alloys (TZM).

Mechanical test controlling system comprises of one Microconsole (MTS 458.20), one MicroProfiler (MTS 458.91), one AC controller (MTS 458.13), and two DC controller (MTS 458.11). The MicroProfiler has 52 KB memory and can store ninety nine programs. Remote programmability allows the programs to be sent from computer via RS 232. Signals from the load cell, extensometer, or LVDT can be used to perform the load, strain, or stroke tests.

The Centorr Model S-60 high vacuum furnace is mounted on the load frame of MTS. Two bellows for the 50.8 mm diameter rods accommodates the movements of the actuator up to 150 mm. The hot zone size is 76.2 mm diameter by 203.2 mm high with two halves of tungsten mesh heating elements. The heat radiations are blocked by six layers of heat shields made of tungsten and molybdenum. The extensometer is fixed in the furnace chamber outside the heat shields. Fig. 16. [35] shows the final set up for the test. The maximum operating temperature of the furnace is 2000°C in vacuum or controlled inert gas (argon, nitrogen, helium) atmosphere. Two "C" W5%Re/W26%Re type thermocouples are used along with a 20 segment programmable Honeywell Universal Digital Controller. Three mode controller provides temperature control stability within ±1°C accuracy. Over temperature controller is installed to protect the system from over heating in the case of damaged or broken main thermocouple.

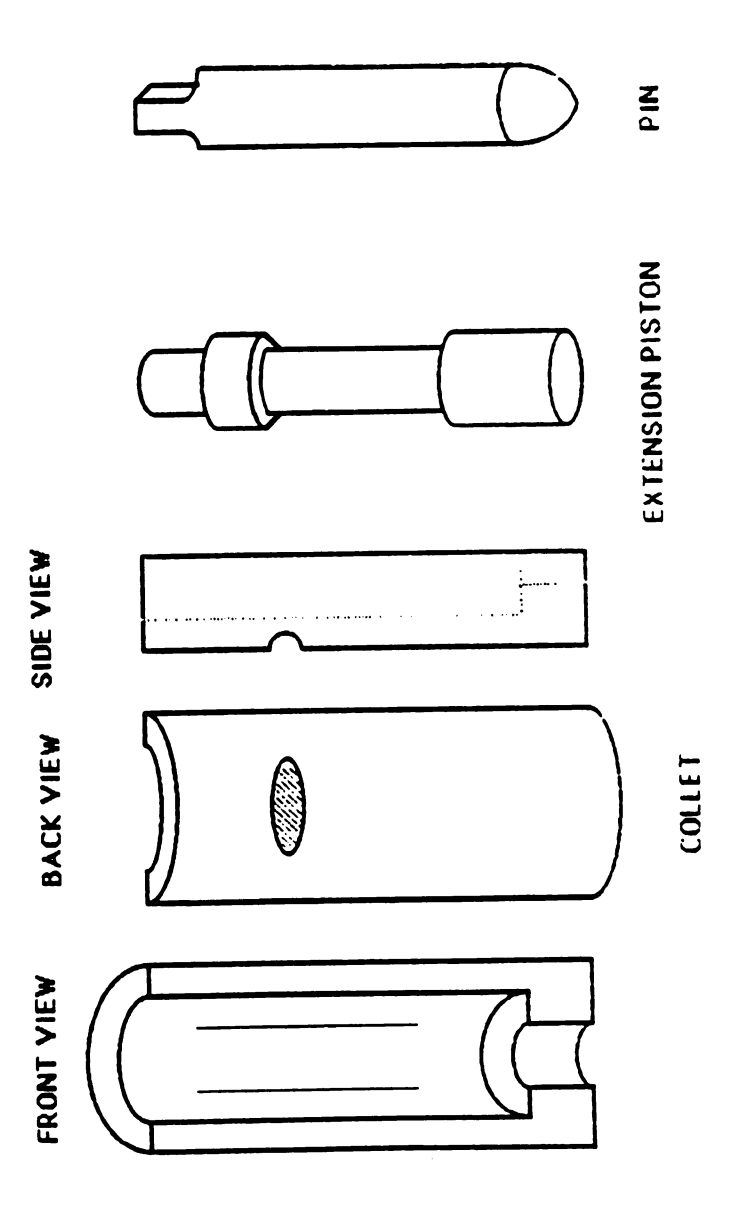


Fig. 15. Specimen inserts for the high temperature high vacuum MTS test system [35].

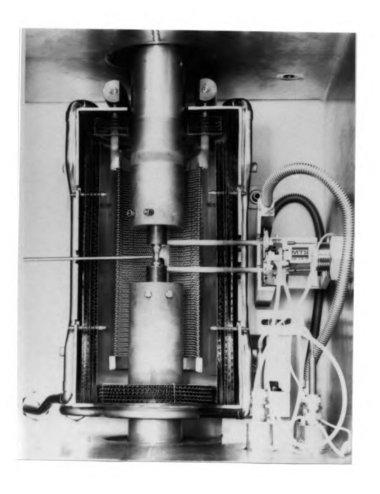


Fig. 16. Final set up inside the vacuum furnace of the high temperature high vacuum MTS test system [35].

Machine control and data acquisition is performed by a Zenith AT personal computer with 1MB main memory. One high performance A/D Input Output board (Data Translation DT 2818) is connected to the one of the expansion slots of the personal computer. The DT 2818 can be programmed from the computer compiled BASIC language to perform A/D conversions, D/A conversions, and digital input and digital output transfers. It has a 12 bit A/D converter with a maximum data sampling rate of 13.7 kHz. Using Direct Memory Access (DMA), the data can be moved directly into or out of BASIC variable arrays at high speeds. PCLAB, a real-time application software package containing a number of machine language routines designed to be called from computer compiled BASIC language greatly reduced the programming required to use DT 2818. High level routines for data acquisition and control were written by Chen [35] in MicroSoft QuickBASIC language.

4. EXPERIMENTAL RESULTS

4.1 Mechanical Behavior

In order to characterize the high temperature deformation at 600° C, two strain amplitudes (elastic + plastic) of 0.5% and 1% were used. A plot of true stress versus cumulative strain, obtained from a test conducted in high vacuum using 0.5% strain amplitude, is shown in Fig. 17. In the first few cycles, the true stress rapidly increased before reaching saturation, then decreased in the latter cycles. The initial steep increase in the true stress was due to large strain hardening rate. The subsequent decrease in the true stress at large cumulative strain indicates the occurrence of a strong softening mechanism. Fig. 18 exhibits results corresponding to 1% strain amplitude cyclic test, using a reducing (90% N_2 + 10% H_2) atmosphere. This test also shows a maximum followed by a continuous decrease in the true stress. Fig. 19 is a plot of the true stress versus the number of cycles for 1% strain amplitude cyclic test, using a reducing (90% N_2 + 10% H_2) atmosphere. It corroborates the true stress behavior represented by Fig. 18. Fig. 20 shows the results of stress controlled test (constant stress of 85 MPa) in a reducing (90% N_2 + 10% H_2) atmosphere.

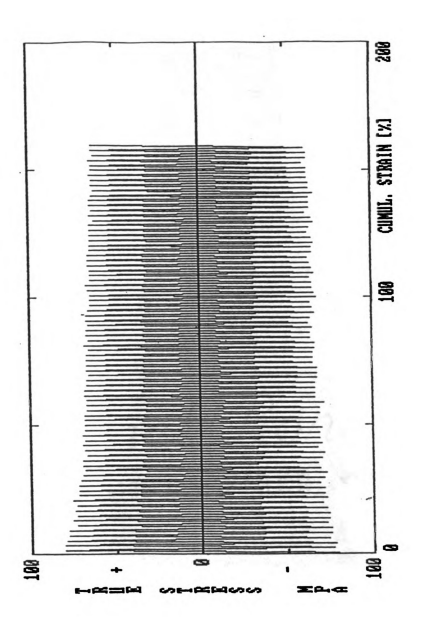


Fig. 17 Plot of true stress versus cumulative strain for 0.5% strain amplitude cyclic deformation in high vacuum at $600^{\rm O}{\rm C}$.

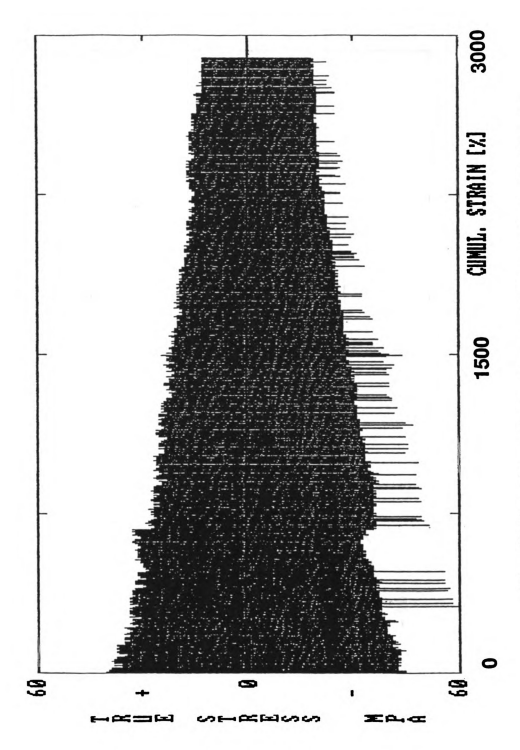


Fig. 18 Plot of true stress versus cumulative strain for 1% strain amplitude cyclic deformation in reducing atmosphere of (90% $N_2+10\%$ H_2) at 600°C.

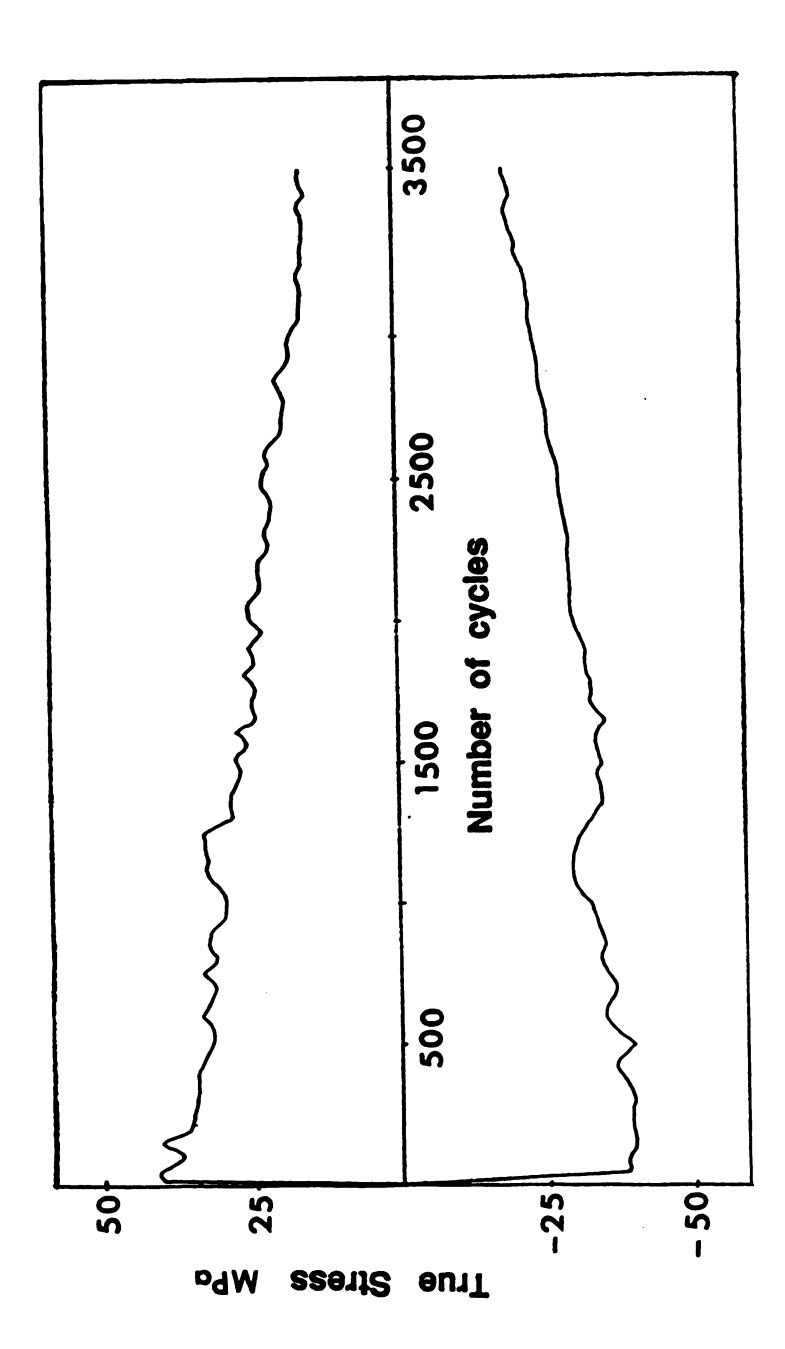


Fig. 19 Plot of true stress versus number of cycles for 1% strain amplitude cyclic deformation in reducing atmosphere of (90% N_2 + 10% H_2) at 600°C.

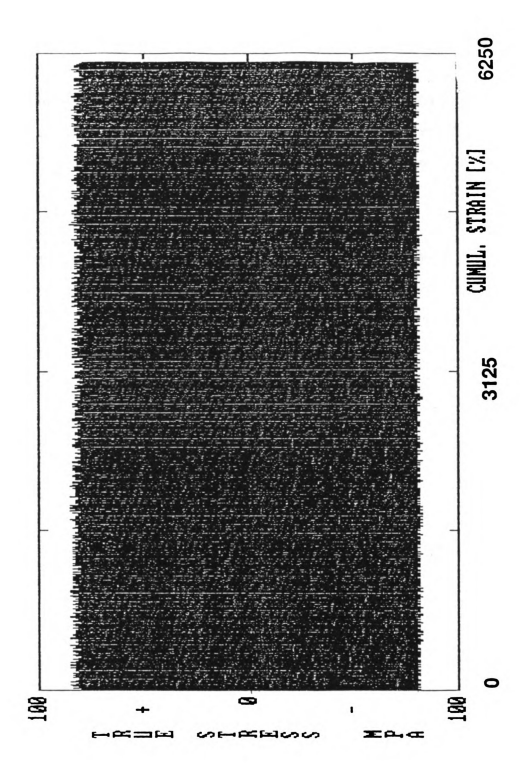


Fig. 20 Plot of true stress versus cumulative strain for constant stress controlled test, using constant stress of 85 MPa, in reducing atmosphere of (90% $N_2+10\%$ $H_2)$ at 600^0 C.

4.2 Microstructural Development

Substantial differences were observed in the microstructure of the specimens in the initial and final states. A very few large grains are observed in Fig. 21 (0.5% strain amplitude cyclic loading in vacuum) as compared to Fig. 11 (initial structure). Extensive grain boundary migration can be observed by comparing Fig. 10 (initial microstructure) to Fig. 22 (after 1% strain amplitude cyclic test). Similar microstructural changes can be observed by comparing Fig. 23 (initial microstructure) to Fig. 24 (after stress controlled test). However, one high temperature test done in vacuum did not show any significant microstructural change even after 1000 cycles of loading [Figs. 25 and 26].

For a specimen annealed at 800° C for 5 hour and fatigued at 0.5% strain amplitude in high vacuum, the microstructure in the plane parallel to the loading direction showed a tendency of grain boundary alignment at $\pm 45^{\circ}$ to the stress axis [Fig. 27]. Another specimen annealed at 1200° C for 2 hour and fatigued at 0.5% strain amplitude in high vacuum, showed no such tendency [Fig. 28].

4.3 Brittle Failure

The fractured surface of a specimen that broke in 0.5% strain amplitude cyclic test in a reducing (90% $N_2 + 10\% H_2$) atmosphere showed extensive intergranular cleavage with a very little transgranular fracture (Figs. 29 and 30).

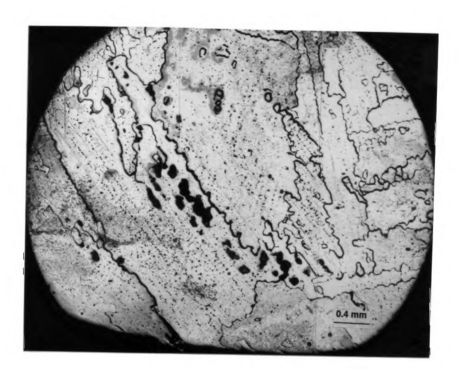


Fig. 21 Microstructure of Ni $_3$ Al, in the plane perpendicular to the loading axis, annealed at 800^0 C for 5 hour, after 100 cycles of 0.5% strain amplitude at 600^0 C.



Fig. 22 Microstructure of Ni $_3$ Al, in the plane perpendicular to the loading axis, annealed at 800^0 C for 5 hour, after 3900 cycles of 1% strain amplitude at 600^0 C.

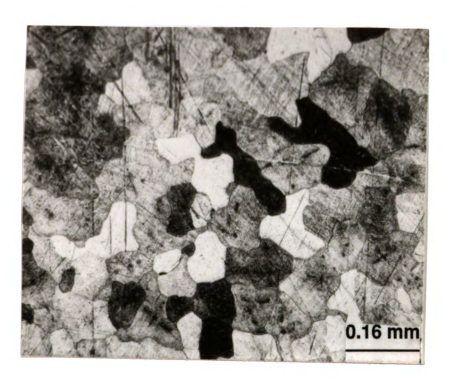


Fig. 23 Microstructure of Ni $_3{\rm Al},$ in the plane perpendicular to the loading axis, annealed at 800^0C for 5 hour.

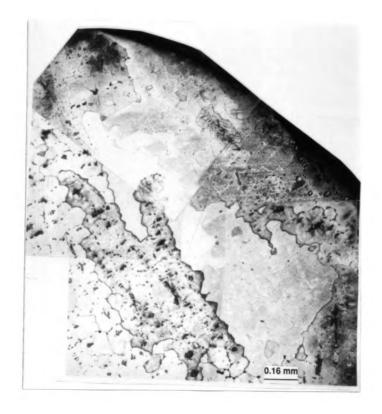


Fig. 24 Microstructure of Ni $_3$ Al, in the plane perpendicular to the loading axis, annealed at 800^0 C for 5 hour, after 790 cycles of constant stress of 85 MPa at 600^0 C.



Fig. 25 Microstructure of Ni $_3\text{Al},$ in the plane perpendicular to the loading axis, annealed at 1200^0C for 2 hour.

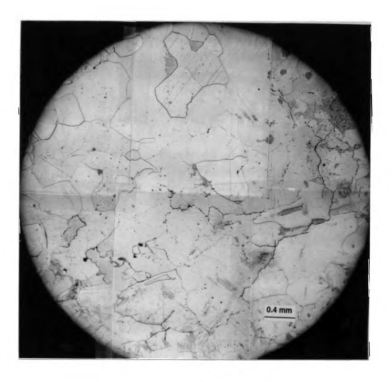


Fig. 26 Microstructure of Ni_3Al , in the plane perpendicular to the loading axis, annealed at 1200^9C for 2 hour, after 1000 cycles of 0.5% strain amplitude at 600^9C .

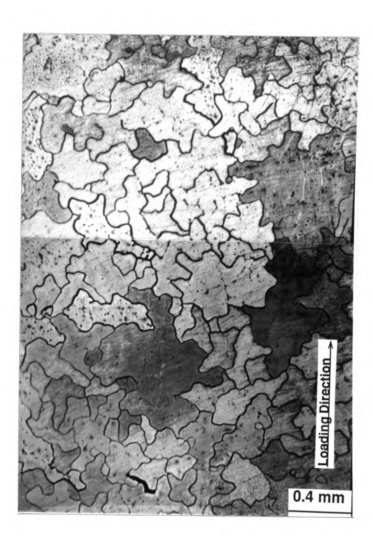


Fig. 27 Microstructure of Ni $_3Al,$ in the plane parallel to the loading axis, annealed at 800^0C for 5 hour, after 100 cycles of 0.5% strain amplitude at $600^0C.$

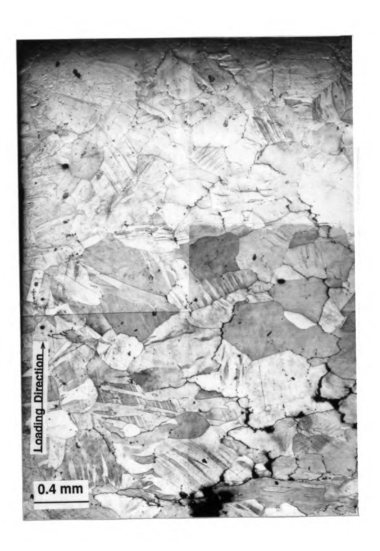


Fig. 28 Microstructure of Ni $_3$ Al, in the plane parallel to the loading axis, annealed at 1200^o C for 2 hour, after 1000 cycles of 0.5% strain amplitude at 600^o C.

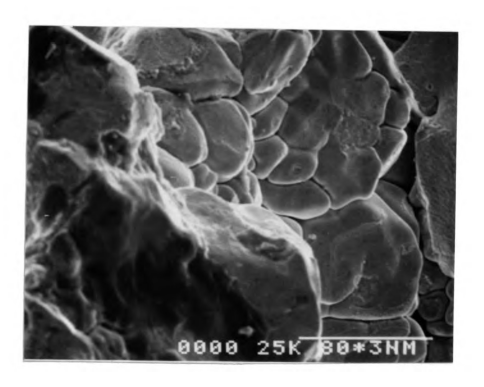


Fig. 29 SEM micrograph of the fractured surface of a specimen broken during cyclic loading in the (90% $N_2+10\%\ H_2$) atmosphere.

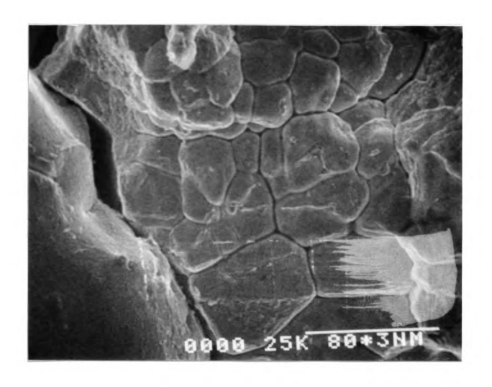


Fig. 30 SEM micrograph of the fractured surface of a specimen broken during cyclic loading in the (90% $N_2+10\%\ H_2$) atmosphere.

5. DISCUSSION

5.1 Mechanical Behavior

All the cyclic hardening curves [Figs. 17-20] show a maximum followed by a continuous decrease in the true stress. The nature of curve remains same for different strain amplitudes and stress controlled test. The continuous decrease in the true stress after the maximum indicates the occurrence of a strong mechanism at large cumulative strain. The softening could be due to the grain boundary migration.

5.2 Grain Boundary Migration

Extensive grain boundary migration was found in all but one cyclic tests. Grain boundary migration during LCF has been reported in Al[16,17,30], Pb[14,15], Pb-Sn solid solution alloy[31,32], Al-Mg solid solution alloy[33], and Ni[18].

No evidence of grain boundary migration in one of the test [Figs. 25,28] could be attributed to the voids present in that particular specimen [Fig. 28].

Dispersions like precipitates and voids pin down the grain boundaries thus inhibit the grain boundary migration.

5.3 Brittle Failure

Liu and White [2] have reported oxygen embrittlement of B-doped polycry-stalline Ni₃Al during the high temperature deformation. The sample observed under SEM had clean grain boundary cleavage with a very little ductile fracture. Although a reducing mixture of $(90\% N_2 + 10\% H_2)$ was used in the Instron machine, the presence of the traces of air could not be ruled out. The brittle failure could be attributed to the presence of elemental oxygen at the grain boundaries and/or formation of glassy B₂O₃ phase.

6. CONCLUSIONS

The present study on B-doped Ni₃Al yields the following results:

- 1. Under high temperature low cycle fatigue, the true stress amplitude (as a function of the cumulative strain) shows a maximum, followed by a continuous decrease at large cumulative strains.
- 2. There is an extensive grain boundary migration during the high temperature low cycle fatigue.
- 3. Dispersions in the form of voids, pin down the grain boundaries and inhibit grain boundary migration.
- 4. The ductility of B-doped Ni₃Al strongly depends on the test environment.

 Oxygen, if present even in traces, adversely affects the ductility of the material.

7. BIBLIOGRAPHY

- [1] M. Hansen, Constitution of Binary Alloys, McGraw Hill Book Co., New York, p. 119, (1958).
- [2] C. T. Liu and C. L. White, Acta Metall., vol. 35, No. 3, pp. 643-649, (1987).
- [3] P. H. Thorton, R. G. Davis and T. L. Johnson, Metall. Trans. 1 p. 207, (1977).
- [4] P. A. Flinn, Trans. TMS. AMIE 218, p. 145, (1960).
- [5] R. G. Davis and N. S. Stoloff, Trans. TMS. AMIE 233, p. 714, (1965).
- [6] E. M. Grala, Mechanical Properties of Intermetallic Compounds, ed. J. H. Westbrook, John Wiley and Sons, Inc., New York, p. 358, (1960).
- [7] R. Moskovic, J. Mater. Sci. 13, p. 1901, (1978).
- [8] K. Aoki and O. Izumi, Trans JIM 19, p. 203, (1978).
- [9] A. V. Seybolt and J. H. Westbrook, Acta Metall. 12, p. 449, (1964).
- [10] K. Aoki and O. Izumi, Nippon Kinzoku Gakkaishi 41, p. 170, (1977).
- [11] C. T. Liu and C. C. Koch, Technical Aspects of Critical Materials Used by the Steel Industry, vol. IIB, NBSIR-83-26-A-Z, National Bureau of Standards, p. 42-1, (1983).
- [12] C. T. Liu, C. L. White and J. A. Horton, Acta Metall., vol. 33, p. 213, (1985).
- [13] A. I. Taub, S. C. Huang and K. M. Chang, private communication (1984).

- [14] T. G. langdon and R. C. Gifkins, Acta Metall., vol. 31, pp. 927-938, (1983).
- [15] T. G. langdon, D. Simpson and R. C. Gifkins, Acta Metall., vol. 31, pp. 939-946, (1983).
- [16] P. Yavari and T. G. langdon, Acta Metall., vol. 31, pp. 1595-1603, (1983).
- [17] P. Yavari and T. G. langdon, Acta Metall., vol. 31, pp. 1605-1610, (1983).
- [18] S. R. Chen and G. Gottstein, Acta Metall., vol. 36, pp. 3093-3101, (1988).
- [19] C. T. Liu and C. L. White, Design of ductile polycrystalline Ni₃Al alloys, (in the press).
- [20] E. M. Schulson and J. A. Roy, Acta Metall., vol. 26, p. 29, (1978).
- [21] S. Takeuchi and E. Kuramuto, Acta Metall., vol. 26, p. 415, (1973).
- [22] C. T. Liu, C. L. White, C. C. Koch and E. H. Lee, High Temperature Materials Chemistry -II, Munir & Cubicciotti, eds, vol 83(7), pp. 32-41, (1983).
- [23] T. Takasugi, E. P. George, D. P. Pope and O. Izumi, Scripta Metallurgica, vol 19, pp. 551-556, (1985).
- [24] T. Ogura, S. Hanada, T. Masumoto and O Izumi, Metallurgical Transactions A, vol 16A, pp. 441-443, (March 1985).
- [25] K. Aoki and O. Izumi, Nippon Kinzoku Gakkaishi 43, p. 1190, (1979).
- [26] E. M. Schulson, T. P. Weihs, I. Baker, H. J. Frost and J. A. Horton, Acta Metall., vol. 34, p. 1395, (1986).
- [27] E. M. Schulson, T. P. Weihs, I. Baker, H. J. Frost and J. A. Horton, Scripta Metall., vol. 19, pp. 1497-1498, (1985).
- [28] E. M. Schulson, I. Baker, H. J. Frost, Metallurgical Transactions A, vol 18A, p. 1995, (Nov. 1985).

- [29] K. U. Snowden, Phil. Mag., vol. 6, p. 321, (1961).
- [30] V. Raman and T. G. langdon, J. Mat. Sci. Lett., vol 2, p. 180, (1983).
- [31] H. S. Betrabet and V. Raman, Metall. Trans., vol. 19A, p. 1437, (1988).
- [32] V. Raman and T. C. Reiley, Scripta Meta., vol. 20, p. 1343, (1986).
- [33] V. Raman and T. G. langdon, Acta Metall., vol. 37, p. 725, (1989).
- [34] H. Abdel-Raouf, A. Plumtree and T. H. Topper, Metall. Trans., vol. 5, p. 267, (1974).
- [35] S. R. Chen, Ph. D. thesis, Michigan State University, (1989).

